https://doi.org/10.5194/tc-2021-1
Preprint. Discussion started: 28 January 2021

The Cryosphere Discussions

Downhole distributed acoustic seismic profiling at Skytrain Ice Rise, West Antarctica

Alex M. Brisbourne[1], Michael Kendall[2], Sofia-Katerina Kufner[1], Thomas S. Hudson[2] and Andrew M. Smith[1],

[1]IDP, NERC British Antarctic Survey, Cambridge, CB3 0ET, UK
[2]Department of Earth Sciences, University of Oxford, Oxford, OX1 3AN, UK

Correspondence to: Alex M Brisbourne (aleisb@bas.ac.uk)

Abstract. Antarctic ice sheet history is imprinted in the structure and fabric of the ice column. At ice rises, the signature of ice flow history is preserved due to the low strain rates inherent at these independent ice flow centres. We present results from a distributed acoustic sensing (DAS) experiment at Skytrain Ice Rise in the Weddell Sea Sector of West Antarctica, aimed at delineating the englacial fabric to improve our understanding of ice sheet history in the region. This pilot experiment demonstrates the feasibility of an innovative technique to delineate ice rise structure. Both direct and reflected P- and S-wave energy, as well as surface wave energy, are observed using a range of source offsets, i.e., a walkaway vertical seismic profile (VSP), recorded using fibre optic cable. Significant noise, which results from the cable hanging untethered in the borehole, is modelled and suppressed at the processing stage. At greater depth, where the cable is suspended in drilling fluid, seismic interval velocities and attenuation are measured. Vertical P-wave velocities are high (V_{INT} = 4029 ± 244 m s^{-1}) and consistent with a strong vertical cluster fabric. Seismic attenuation is high (Q_{INT} = 75 ± 12) and inconsistent with previous observations in ice sheets over this temperature range. The signal level is too low, and the noise level too high, to undertake analysis of englacial fabric variability. However, modelling of P- and S-wave traveltimes and amplitudes with a range of fabric geometries, combined with these measurements, demonstrates the capacity of the DAS method to discriminate englacial fabric distribution. From this pilot study we make a number of recommendations for future experiments aimed at quantifying englacial fabric to improve our understanding of recent ice sheet history.

1 Introduction

Uncertainties in sea level rise projections are dominated by our understanding of how the ice sheets will evolve under a warming climate (IPCC, 2013). Satellite observations over the last 40 years have highlighted the rate of ongoing ice sheet change (Shepherd et al., 2018; Rignot et al., 2019). However, knowledge of past ice sheet change is key to reducing uncertainty in projections of the future behaviour of the ice sheets (Siegert et al., 2019). One key region of West Antarctica where consensus on ice sheet history is yet to be reached is the Weddell Sea sector. Contradictory and incompatible recent histories have been proposed. Hillenbrand et al. (2014) reviewed geological observations as well as marine and terrestrial chronological data and proposed a monotonic ice sheet retreat since the last Glacial Maximum (LGM) to the current grounding line position. However, studies utilising airborne radar surveys (Siegert et al., 2013), ground-based radar and radiocarbon dating (Kingslake et al., 2018) and ice sheet modelling (Bradley et al., 2015) support ice sheet retreat from the LGM to beyond the current grounding line configuration followed by a more recent re-advance. Due to a paucity of absolute dating control, the timing of these changes is also poorly constrained.

Significantly, these contradictory histories imply different stability regimes of the ice sheet in its current configuration, with important implications for a much discussed process, the marine ice sheet instability mechanism, or MISI (Mercer, 1978). MISI describes a feedback mechanism whereby ice streams resting on a reverse bed slope (i.e., deepening upstream) accelerate during retreat. The instability results from an increase in flux at the grounding line as the bed deepens and ice thickness at the grounding line increases as the ice stream retreats. In the Weddell Sea Sector, both the Institute and Möller Ice Streams, for

https://doi.org/10.5194/tc-2021-1
Preprint. Discussion started: 28 January 2021

example, rest on a bed which deepens upstream (Ross et al., 2012). An ice sheet history with monotonic retreat indicates that the current ice sheet configuration may be unstable, with MISI potentially underway. On the contrary, an ice sheet history that includes retreat beyond the current grounding line position with subsequent re-advance to the present-day position demonstrates that the MISI process may be stabilised. For example, in the Amundsen Sea Sector, geodetic observations and modelling results demonstrate that the solid-Earth response to rapid ice loss may result in the stabilisation of retreat (Barletta et al., 2018; Larour et al., 2019).

Ice flow at ice rises (independent ice-flow centres) is gravitationally driven and consequently slow and predictable. As a result, ice rises preserve recent ice flow history within the structure and crystal orientation fabric of the ice column (Kingslake et al., 2016; Brisbourne et al., 2019; Wearing and Kingslake, 2019). Gravity driven flow at ice divides results in the formation of characteristic fabric within the ice column due to the anisotropic nature of ice crystals (Martin et al., 2009). The time taken to reach a steady state, where a characteristic fabric is established, is dependent on a number of factors, including accumulation rate and bed geometry. Deviation from this characteristic fabric indicates change in the ice flow regime and can be used to understand recent ice flow history (Brisbourne et al., 2019).

Surface and airborne geophysical methods provide observations used to constrain likely ice flow history (e.g. Siegert et al., 2013; Bingham et al., 2015; Wearing and Kingslake, 2019). However, as with all surface geophysics measurements, ambiguities in interpretation exist. One method of reducing ambiguity is to make measurements at depth within the ice column, such as a vertical seismic profile (VSP), where seismic receivers are located in a borehole and seismic sources at the surface. Unfortunately, direct access to the deep ice column is logistically difficult, expensive and risky. However, large-scale ice core or hot water drilling experiments potentially provide access to the subsurface as a by-product of the objectives of the primary experiments. It is also now common practice to deploy fibre optic cables downhole to measure temperature profiles within the ice column (Distributed Temperature Sensing, DTS). Distributed acoustic sensing (DAS) provides an opportunity to exploit this existing infrastructure to make additional downhole measurements at little extra cost and minimal risk.

DAS involves measuring the Rayleigh backscattered returns along optical fibre cables. Time-varying strain of the fibre, such as that from passing seismic waves, is derived from changes in the phase difference in backscattered light from closely spaced points along the fibre. The phase-lags measured by an interrogator at the surface are used to reconstruct the seismic record of the subsurface (Hartog, 2017). Such records are analogous to standard seismic methods but measure strain rate rather than velocity, as is the case with standard geophone sensors. The distributed nature of the Rayleigh scatterers within the fibre emulates a continuous subsurface geophone string.

To our knowledge, DAS technology has been deployed only twice previously in glaciological studies, and never in Antarctica. Booth et al. (2020) presented results from an active seismic experiment with borehole deployment of DAS on Store Glacier, West Greenland. Measurements of englacial seismic velocity and attenuation, as well as sub-glacial reflections demonstrated the potential of the DAS method in glaciological settings. Using a deployment of fibre optic cable on an alpine glacier surface, Walter et al. (2020) demonstrated the capacity of the method to record naturally occurring glacial seismicity, and demonstrated the capacity for these observations to locate icequakes and delineate physical properties of the glacier and its bed. We present results from the first field deployment of DAS in an Antarctic borehole. We occupied a recent ice core site to evaluate the potential of DAS technology to constrain the seismic structure of the ice column at an Antarctic ice rise with the aim of improving understanding of ice sheet history. We demonstrate the capability of the method in such scenarios with field observations, highlight the potential for the method to discriminate englacial structure through modelling, and make recommendations for future deployments in similar situations.

https://doi.org/10.5194/tc-2021-1
Preprint. Discussion started: 28 January 2021

2 Field setting and data acquisition

Skytrain Ice Rise (SIR) in the Weddell Sea region of West Antarctica is an independent ice flow centre adjacent to the Filchner-Ronne Ice Shelf, bounded by the fast-flowing Rutford and Institute Ice Streams, Constellation and Hercules Inlets, and the southern end of the Ellsworth-Whitmore Mountains (Fig. 1a,b). In 2018/19, as part of the WACSWAIN Project (Mulvaney et al., 2020), an ice core was recovered to bedrock at 651 m depth close to the highest point of the ice rise (Fig. 1b). The experiment site is directly above a Raymond Bump visible in radar profile data (Mulvaney et al., 2020), indicative of long-term stable ice flow. Surface ice flow speed is < 10 m a^{-1} (Rignot et al., 2011). Following extraction of the ice core, three cables were deployed in the borehole: (1) a thermistor string to a depth of 635 m with instruments at known depths (635, 585, 535, 385 and 235 m); (2) a PT-100 platinum resistance thermometer to 95 m depth, and (3) a multimode fibre optic cable to 595 m depth, principally for DTS. The three cables were joined at 5 m intervals. The borehole remained open due to a combination of slow ice flow at the ice divide and the presence of drilling fluid in approximately the lower half of the borehole (exact depth unknown).

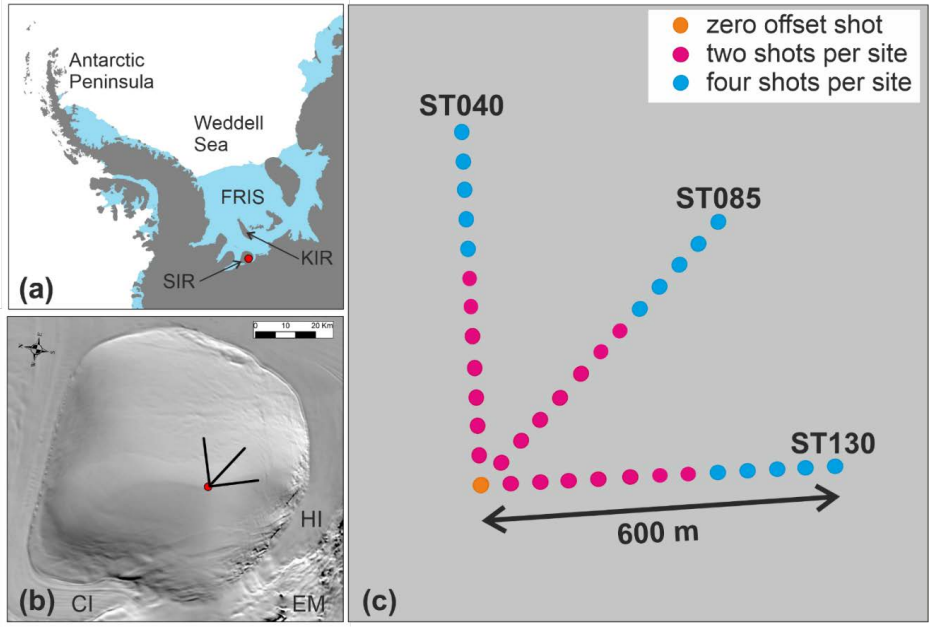

Figure 1: (a) Location of the experiment (red dot) on SIR in West Antarctica. FRIS – Filchner-Ronne Ice Shelf; KIR – Korff Ice Rise. (b) Orientation of walkaway hammer and plate seismic lines on Skytrain (not to scale). The background is MODIS imagery (Scambos et al., 2007). HI – Hercules Inlet; CI – Constellation inlet; EM – Ellsworth-Whitmore Mountains. (c) Scale map of shot locations with respect to the borehole (orange dot). Line names reference the orientation with respect to magnetic north.

In January 2020 the site was revisited to conduct a VSP experiment centred on the borehole using a Silixa iDAS^{TM} interrogator unit with GPS timing. A 1.0 kVA petrol generator was used to power the interrogator unit. The interrogator was housed in a tent to protect it from the wind and maintain a working temperature. Data were recorded at 8000 Hz sampling frequency. Strain rate measurements were made at 1 m intervals along the fibre but with an effective resolution of 10 m due to the "gauge length" or strain rate averaging process (Dean et al., 2017). The fibre optic cable includes a bend at 595 m, where an identical length of fibre within the cable is spliced and returned to the surface, enabling two measurements to be made at each depth. The DAS

https://doi.org/10.5194/tc-2021-1
Preprint. Discussion started: 28 January 2021

method measures longitudinal strain. Therefore, with the fibre optic cable vertical, only the vertical strain component of seismic waves propagating past the fibre is measured. Consequently, the cable is sensitive to vertically propagating P-waves but not vertically propagating S-waves.

The acquisition geometry is presented in Figure 1c. With the aim of discriminating anisotropic structure within the ice column, three walkaway profiles were acquired at 45° to one another. Line names reference the orientation with respect to magnetic north. A 4.5 kg sledgehammer with a rigid polyethylene impact plate stamped into the snow surface acted as the energy source. Profiles were acquired out to 600 m offset from the borehole with hammer blows at 50 m intervals. Two hammer blows were made at each shot point out to 350 m and four hammer blows from 400 m and beyond. The interrogator unit recorded in continuous mode with shot gathers subsequently extracted using times derived from impulsive arrivals on a continuous 1000 Hz sampled geophone recording made adjacent to the hammer plate.

3 Observations and data processing

Figure 2 presents example VSP records for individual hammer blows at a range of offsets along line ST130. Data are "folded" about the bend in the cable, resulting in a stack of two traces for each hammer blow. Figure 2a presents the zero offset or "checkshot" (i.e., source at the top of the borehole) bandpass filtered at 2-140 Hz. The downwards propagating P-wave, the primary ice base reflection and the surface multiple are all visible. The primary downwards-propagating P-wave arrival is disrupted at around 350 m depth. A mixture of upgoing and downgoing energy is observed at 100-300 m depth following the primary P-wave arrival, producing a diamond-shaped signal pattern on a depth-time plot. From zero to 150 ms, prior to the primary P-wave arrival, a horizontal signal is observed in Figure 2a. A signal which plots horizontally in a VSP indicates an arrival coincident in time along the length of the fibre optic cable. This is however unlikely in this situation and is most likely due to vibration of the interrogator unit, a result of wind and generator noise at the surface.

https://doi.org/10.5194/tc-2021-1
Preprint. Discussion started: 28 January 2021

The Cryosphere Discussions
Open Access
EGU

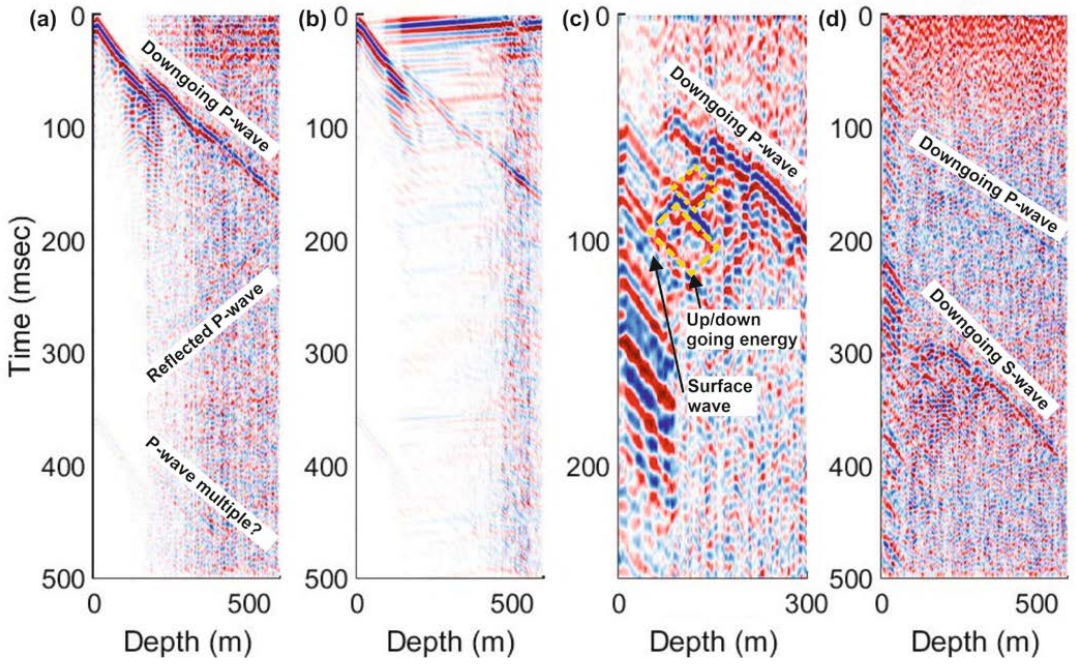

Figure 2: Example DAS VSPs along line ST130 with signal and noise labelled. Traces are normalised at each depth to highlight coherent arrivals. (a) Primary, reflected and surface-multiple P-waves at zero offset with a bandpass filter of 2-140 Hz; (b) Downgoing P-wave energy at zero offset isolated using an F-K filter and adaptive deconvolution to remove upgoing energy and reduce coherent noise; (c) Detail (0-300 m depth; 0-250 ms only) of a source at 100 m offset with a bandpass filter of 2-140 Hz. The characteristic diamond-pattern is highlighted by yellow-dash boxes; (d) Both P-wave and S-wave arrivals are visible at 500 m offset with bandpass filter of 2-140 Hz applied.

Figure 2b presents the checkshot record as presented in Figure 2a, but with a frequency-wavenumber (FK) filter applied to suppress upward propagating seismic energy (negative wavenumber energy removed, 2-140 Hz bandpass) and with an adaptive deconvolution filter (Griffiths et al., 1977) applied to remove coherent noise. The upgoing energy is removed, but the primary P-wave energy remains discontinuous with the wavetrain disrupted. The combined up-downgoing signal at approximately 100-300 m depth is suppressed by the combination of the FK and adaptive deconvolution filters. However, some upgoing energy persists at depths of less than 300 m. Over a shorter time interval and shallower depth range, Figure 2c presents details of the VSP record acquired with a shot offset of 100 m on line ST130. A 2-140 Hz bandpass filter is applied. Again, the downgoing P-wave energy is clear, with a delay due to the source offset from the fibre. Relatively high-amplitude but low-frequency energy is present to depths of 100 m. The characteristic diamond pattern is again observed, to a depth of around 300 m, indicating both up and down-going energy. Figure 2d presents the VSP with a shot offset of 500 m and a 2-140 Hz bandpass filter applied. At this offset, seismic waves propagate more horizontally. Therefore, downgoing S-wave energy dominates the record with downgoing P-wave energy only visible beyond approximately 400 m depth.

3.1 Noise sources

Figure 3a presents a single VSP from a 150 m shot offset along line ST130. The downgoing P-wave is visible at depths below 200 m and the downgoing S-wave at 100 to 200 m. A low frequency signal is also visible at times greater than 180 ms and

https://doi.org/10.5194/tc-2021-1
Preprint. Discussion started: 28 January 2021

from the surface to a depth of 100 m. As described above, significant noise is present on the records at depths of less than 300 m. This takes the form of "diamond shapes" indicating a combination of up and downgoing energy. The most obvious source of signals of this type is englacial reflections of downgoing energy. However, a number of factors indicate a different noise source of such signals. The firn column consists of snow compacting and densifying under its own weight to form solid ice, with a pore close off depth at SIR of 56 m (Mulvaney, 2020). Below this depth the ice column likely varies very little at scales sensitive to the seismic wavelengths analysed here ($\lambda \sim 36$ m) and the seismic velocity is predominantly controlled by temperature, which varies slowly. The low temperatures at Skytrain preclude ice layers in the firn. Therefore, there is no likely source of layering which could result in seismic reflections of any significance from within the ice column. Similarly, the stress regime precludes englacial crevassing. No structures are observed in the radar profile collected across SIR (Mulvaney, 2020, Fig. 3).

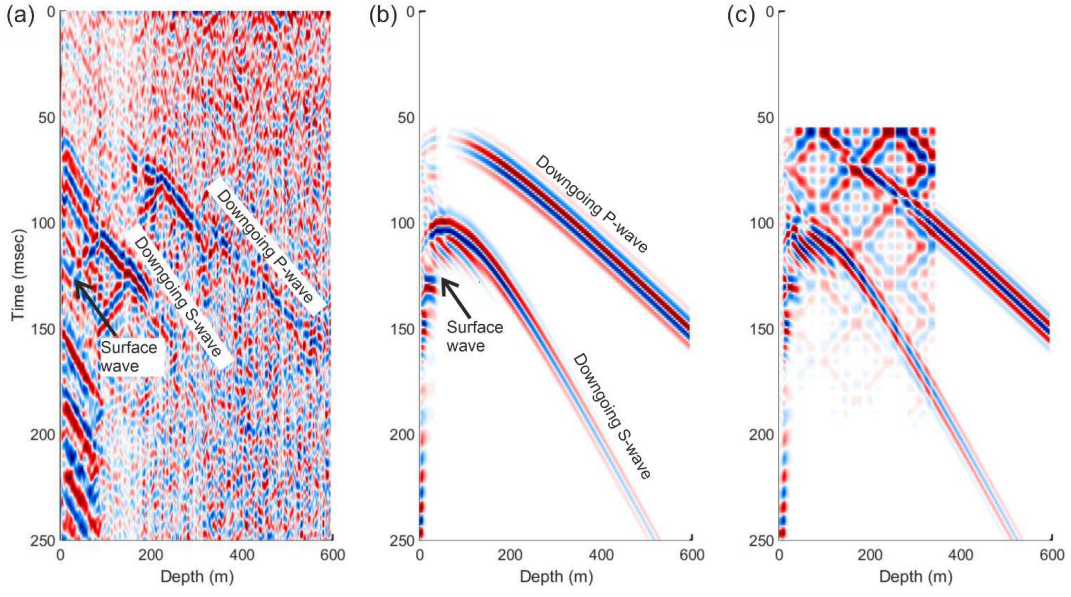

Figure 3: Observed and synthetic VSPs with a shot offset of 150 m from the top of the borehole along line ST130. Traces are normalised at each depth. (a) Observed VSP with a 2-140 Hz bandpass filter applied; (b) Synthetic VSP with the principal arrivals labelled; (c) Synthetic VSP summed with simple harmonic motion of a vibrating string fixed at both ends (0m and 300m).

We therefore propose a different source for the diamond-shaped signal. As stated above, the hole remains open. The fibre optic cable is unlikely to be frozen to the borehole (R. Mulvaney, Pers. Comm.). This is in contrast to the experiment of Booth et al. (2020) where the borehole closed-up within a few days. Prior to close-up of the borehole, Booth et al. (2020) observed a similar diamond-shaped signal pattern in the VSP data. We therefore attribute this noise to the fibre being unclamped in the hole and hanging in air. At depths where the drilling fluid is present (below around 300 m) the fibre optic cable sits in the fluid and couples to the walls of the hole via the fluid. At these depths we can expect lower noise levels due to damping of vibrations of the cable and improved signal coupling. This is indeed the case in our data where we see a transition at around 300 m depth. This depth also coincides with a discontinuity in the primary P-wave arrival, consistently observed over a range of shot offsets and azimuths. The onset of diamond-shaped noise is coincident with the first P-wave arrival, in this case at around 50 ms, and we therefore attribute noise of this form to the excitation of vibrations on the cables by seismic energy passing the borehole.

https://doi.org/10.5194/tc-2021-1
Preprint. Discussion started: 28 January 2021

To test this idea we construct full-waveform synthetics to simulate VSP records with added coherent noise due to cable resonance. Figure 3b shows a synthetic VSP simulating a 150 m offset shot into a 600 m downhole fibre optic cable. We use SPECFEM2D current source (Tromp et al., 2008) published under the CeCILL V2 license. We convert the synthetic seismogram from velocity to strain rate to emulate DAS measurements. We assume the seismic velocity profile as measured at the adjacent Korff Ice Rise (Brisbourne et al., 2019). In this synthetic VSP (Fig. 3b), clear P- and S-wave energy is observed, consistent with the observations. The low frequency surface waves in the synthetic seismogram are coincident with a low frequency arrival in the observations (Fig. 3a). We hypothesise that as it traverses the borehole the surface wave excites a mode of vibration on the fibre that propagates its length. We argue that this signal is not a depth-observation of the surface wave due to slope of the arrival in Figure 2c. A surface wave traversing the fibre would appear coincident along the fibre, i.e. with a horizontal nature in the VSP.

In Figure 3c we present the sum of the synthetic seismogram and a synthetic noise signal generated assuming simple harmonic motion (SHM) on a string of length 340 m fixed at both ends and with nodes at 85 m intervals. These parameters are set at values that produce a reasonable simulation of the observations and are not intended to match the conditions down the borehole, which are poorly constrained. We initiate the synthetic SHM at the arrival time of the P-wave at the borehole and apply exponential decay with time to this signal. The SHM produces the characteristic diamond-shaped signal as observed in the VSPs. The summation of the synthetic seismogram and noise also produces nulls in the resultant direct wavetrain, similar to those observed in the data. The synthetic profile is not an exact representation of the observations. However, similarities with the observations indicate that the most likely source of this diamond-shaped noise is vibrations on the cables suspended in air, initiated by the propagation of the seismic signal past the borehole.

Unfortunately, the effect of cable resonance in the open parts of the borehole render it difficult to use data from this section of the cable in an analysis of seismic properties of the ice column. Hence, we only expect useful results from the cable in the deeper parts of the borehole. To improve signal to noise levels for further data analysis the “folded” shot records are stacked to combine all hammer blows at each shot point.

4 Data analysis and results

4.1 Seismic P-wave velocity

Seismic interval velocities can be calculated from the traveltime through layers of known thickness. Therefore, VSPs at ice rises allow direct measurement of interval velocities through the ice column. The thickness of interval interrogated depends on the trade-off between resolution and noise levels. Prior to velocity analysis we apply an FK filter, passing 2-140 Hz and removing negative wavenumbers to reduce upgoing energy. We also apply an adaptive deconvolution filter to remove coherent noise. We use a sliding window of 50 m length to determine interval velocities along the three azimuths. Within each 50 m window we determine the best linear fit to the traveltime picks and calculate the interval velocity from the gradient. Velocity uncertainties are calculated using the one standard deviation uncertainty of the linear traveltime fit over each 50 m sliding window. The range of velocities over each window is calculated by perturbing the interval traveltime by plus and minus two standard deviations to emulate the maximum possible range of traveltime intervals. As depths are relative, the error in interval length is negligible. Figure 4 presents interval velocities from the 0, 50 and 100 m offset shots. Noise in the upper half of the ice column and the discontinuity in the P-wave arrival at approximately 300 m results in consistent, yet physically unrealistic velocities above 380. Below 540 m depth the sliding window length precludes further measurements. Table 4 presents mean interval velocities between 380 and 540 m shots over the three azimuths and offsets out to 100 m. To convert from apparent

https://doi.org/10.5194/tc-2021-1
Preprint. Discussion started: 28 January 2021

to true velocity we calculate the incidence angle of the wavefront at the vertical fibre optic cable by assuming straight raypaths between the source and centre of the receiver interval.

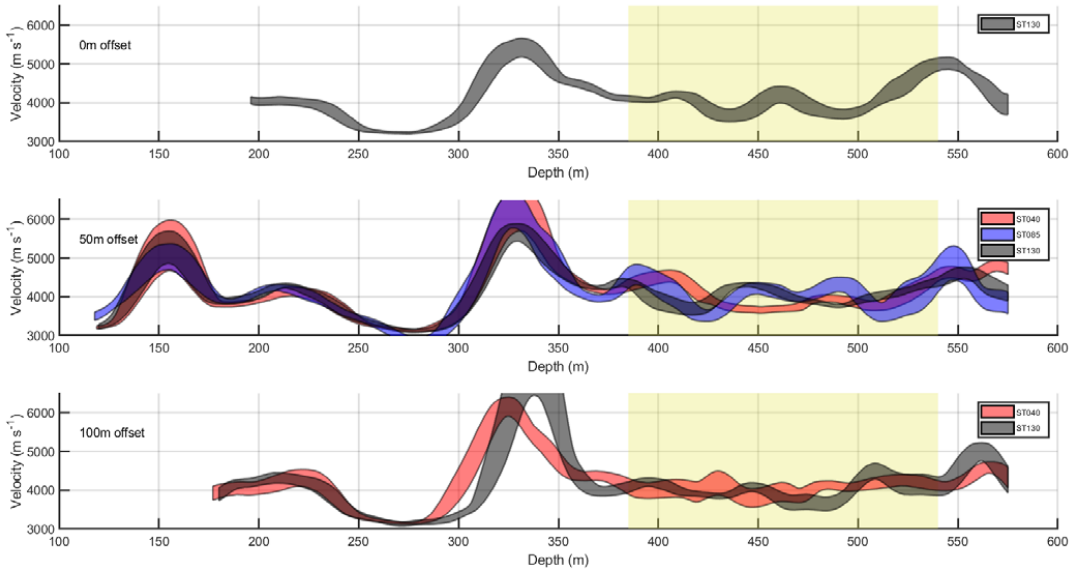

215 **Figure 4: Vertical P-wave velocity from 0 m (upper plot), 50 m (middle plot) and 100 m offset (lower plot) shots calculated using a linear fit to 50 m sliding windows. Velocities are converted from the apparent velocity assuming straight ray paths between the source offset and a receiver at the midpoint of the respective sliding window. The width of the fitted curves represents the velocity uncertainty calculated from the traveltime uncertainty over each sliding window. The yellow box represents the depth range over which mean interval velocity and Q are presented in Table 1 (380 to 540 m depth).**

220

The mean velocity of 4029 ± 244 m s^{-1} is high but comparable to that of Booth et al. (2020) in the deepest part of the ice column of Store Glacier, Greenland. Although uncertainties are large, the inferred high velocities may indicate seismic anisotropy with vertical c-axes, most likely a vertical cluster fabric (Martin et al., 2009; Harland et al., 2013). Uncertainties in the velocity measurement preclude interpretation of fabric from depth or azimuthal variation in P-wave velocity.

225

https://doi.org/10.5194/tc-2021-1
Preprint. Discussion started: 28 January 2021


The Cryosphere Discussions

Table 1 Vertical interval velocities measured between 380 and 540 m depth. Uncertainties are one standard deviation.

Line	Shot offset (m)	V_{INT} (m s^{-1})
ST040	50	4004 ± 283
ST040	100	4049 ± 128
ST085	50	4039 ± 274
ST085	100	-
ST130	0	4056 ± 307
ST130	50	4027 ± 208
ST130	100	4000 ± 216
Mean		**4029 ± 244**

4.2 Seismic attenuation

The spectral ratio method (Bath, 1974) is applied to the direct P-wave arrivals to determine seismic attenuation along vertical propagation paths within the ice column (Figure 5). The natural logarithm of the spectral ratio is determined.

$$ln\left|\frac{A_1(f)}{A_2(f)}\right| = const. + \pi\frac{\delta t}{Q}f \quad (1)$$

The slope of the spectral ratio $m = \pi\frac{\delta t}{Q}$ yields the quality factor.

We apply the spectral ratio method across a single depth interval from 380 to 540 m, consistent with the interval velocity measurements. We use the zero-offset shots to analyse vertical raypaths as a strong dependence of attenuation on crystal orientation has previously been demonstrated (Oguro et al., 1982). To aid phase picking, traces are bandpass filtered at 2-140 Hz. Traces are then windowed around the primary P-wave arrivals. DAS measurements of strain rate implicitly average over a gauge length of 10 m. In addition, at Skytrain, little change is expected in the ice column over a 10 m depth range. Therefore, to improve the signal to noise ratio, traces are stacked over a 10 m window at the respective depths. To remove noisy traces and compensate for the discontinuous nature of the wavetrain, prior to stacking we perform a cross correlation to evaluate each trace against the central trace of the respective interval. Traces with a correlation coefficient < 0.95 are discarded (Fig. 5a-c). To calculate the uncertainty in the gradient measurements the 95% confidence limits of the stacked traces are used, analysing waveforms at the extremes of this envelope (Fig. 5a,b) to calculate a range of spectral ratios and therefore gradients. In addition, the uncertainty in the gradient fit and traveltimes (±1 ms) are used to determine the uncertainty in Q. A mean interval Q of 75 ± 12 for this lower section of the ice column is measured. The uncertainties are consistent with previous studies that use the spectral ratio method (Dasgupta and Clark, 1998; Peters et al., 2012). The temperature measured over this depth range in the ice column is -20° to -17° C (Mulvaney et al., 2020).

https://doi.org/10.5194/tc-2021-1
Preprint. Discussion started: 28 January 2021

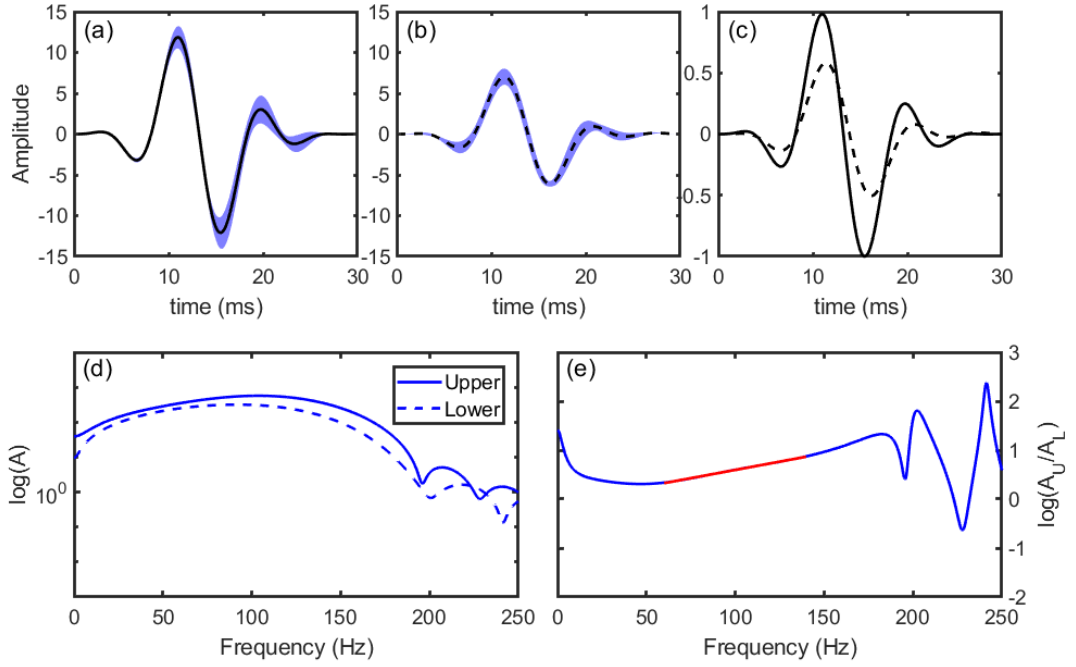

Figure 5: Use of the spectral ratio method to determine seismic attenuation. Traces are stacked around the direct P-wave arrivals over a 10 m interval. The cross-correlation with the central trace in the respective depth window is calculated and only traces with a coefficient > 0.95 are used. (a) Upper stacked trace (solid line) and (b) Lower stacked trace (dashed line), both with 95% confidence bounds calculated from the summed traces in blue; (c) Upper (solid line) and lower (dashed line) stacked traces with normalized amplitude; (d) Amplitude spectra of the upper and lower stacked waveforms. (e) Log spectral ratio with the frequency range over which the gradient is measured in red (60-140 Hz).

5 Evaluating the potential of DAS VSP for ice column fabric discrimination using synthetic traveltimes and amplitudes

Our observations of P- and S-waves, both direct and reflected, and at a range of offsets and azimuths, demonstrate the potential for DAS type measurements at Antarctic ice rises. We therefore investigate the capacity of DAS measurements to discriminate ice column fabric at ice rises to guide future experiments investigating ice sheet history through fabric evolution (e.g., Brisbourne et al., 2019). We use the software package ATRAK (Guest and Kendall, 1993), based on asymptotic ray theory (Kendall and Thomson, 1989), to calculate traveltimes and amplitudes of direct P- and S-wave arrivals from a range of offsets and azimuths. An isotropic seismic velocity profile is used in the firn, derived from a previous seismic refraction experiment at Korff Ice Rise (Brisbourne et al., 2019). We test three models of fabric at ice rises: (1) Isotropic; (2) A model with an isotropic layer over a layer with a strong cluster fabric at depth. Critically, radar methods with collocated source and receiver are insensitive to vertical cluster (or azimuthally invariant) fabrics, and seismic methods provide the only proven geophysical approach to quantify azimuthally invariant fabric; (3) A model based on the ice rise fabric predicted by Martin et al. (2009) with a girdle fabric in the upper ice column (80 to 230 m depth) and a strong cluster fabric at depth (230 m to the ice base). The strength of the girdle fabric and fabric depth transition is based on that observed at Korff Ice Rise by Brisbourne et al. (2019). Amplitudes are derived from the vertical component. In reality, two shear waves will propagate in an anisotropic medium. However, the DAS method with a vertical cable is only sensitive to the vertical component of the P-wave energy or vertically polarised S-wave energy.

https://doi.org/10.5194/tc-2021-1
Preprint. Discussion started: 28 January 2021

Figure 6 presents modelled P- and S-wave traveltimes for a shot offset of 200 m and the vertical amplitudes for shot offsets of 200 and 400 m for the three models of fabric. In the isotropic case (Fig. 6a), as expected, there is no azimuthal variation in traveltime or amplitude. Amplitudes vary with depth, with the relationship dependent on shot offset. This is a result of both raypath geometry due to the strong velocity gradient in the firn and the limitation of the downhole fibre DAS method, which measures only vertical strain rate.

The cluster-only model (Fig. 6b) also exhibits no azimuthal variation in traveltime or amplitude. However, in comparison with the isotropic case a very strong depth dependence of amplitude is observed with strong peaks in amplitude at depth. The depth of the peak in S-wave amplitude is dependent on the offset of the shot: shots at progressively greater offset produce peaks in S-wave amplitude at progressively greater depth. This is a result of the focussing of S-wave energy by the strong cluster fabric in what is a homogeneous but anisotropic medium. This amplitude variation is a diagnostic feature that could be quantified in data acquired with a more energetic seismic source. Relatively strong S-wave arrivals are observed in the far offset data from Skytrain (Fig. 2d) although no attempt is made to quantify amplitude variation due to the low signal to noise level. For the extreme form of this fabric, a single maximum, this focussing produces a triplication or folding in the wavefront, which greatly increases the amplitude at depth (results not presented here). Direct observation of a triplication would only be feasible with very high quality measurements and the strong fabrics, and is likely to be beyond the experimental capability (Baird et al., 2017).

The model with both girdle and cluster fabrics exhibits weak azimuthal variation in S-wave traveltimes. However, strong azimuthal variation in amplitudes is observed with maxima in amplitude at 90° intervals (i.e., a four-fold symmetry). There is also a strong depth dependence of the amplitude maxima, which increases with increasing shot offset. Again, this is a diagnostic phenomenon and indicates the viability of the DAS method to image and constrain englacial fabric.

The presence of a girdle fabric alone would in general result in azimuthal variation in traveltimes. However, in our model the observable effect, especially on P-wave traveltimes, is very small. We attribute this to a combination of a weak girdle fabric and the generally vertical nature of the raypaths. To sample the full breadth of velocities associated with a weak girdle fabric, raypaths close to horizontal are required. Further testing of a model with a strong girdle fabric (opening angle of 5°, not presented here) indicates azimuthal variation in P- and S1-wave traveltime of up to 3 ms, likely larger than measurement uncertainties in good quality data. However, S-wave amplitude variations are significantly greater and as such a more robust indicator of fabric.

https://doi.org/10.5194/tc-2021-1
Preprint. Discussion started: 28 January 2021

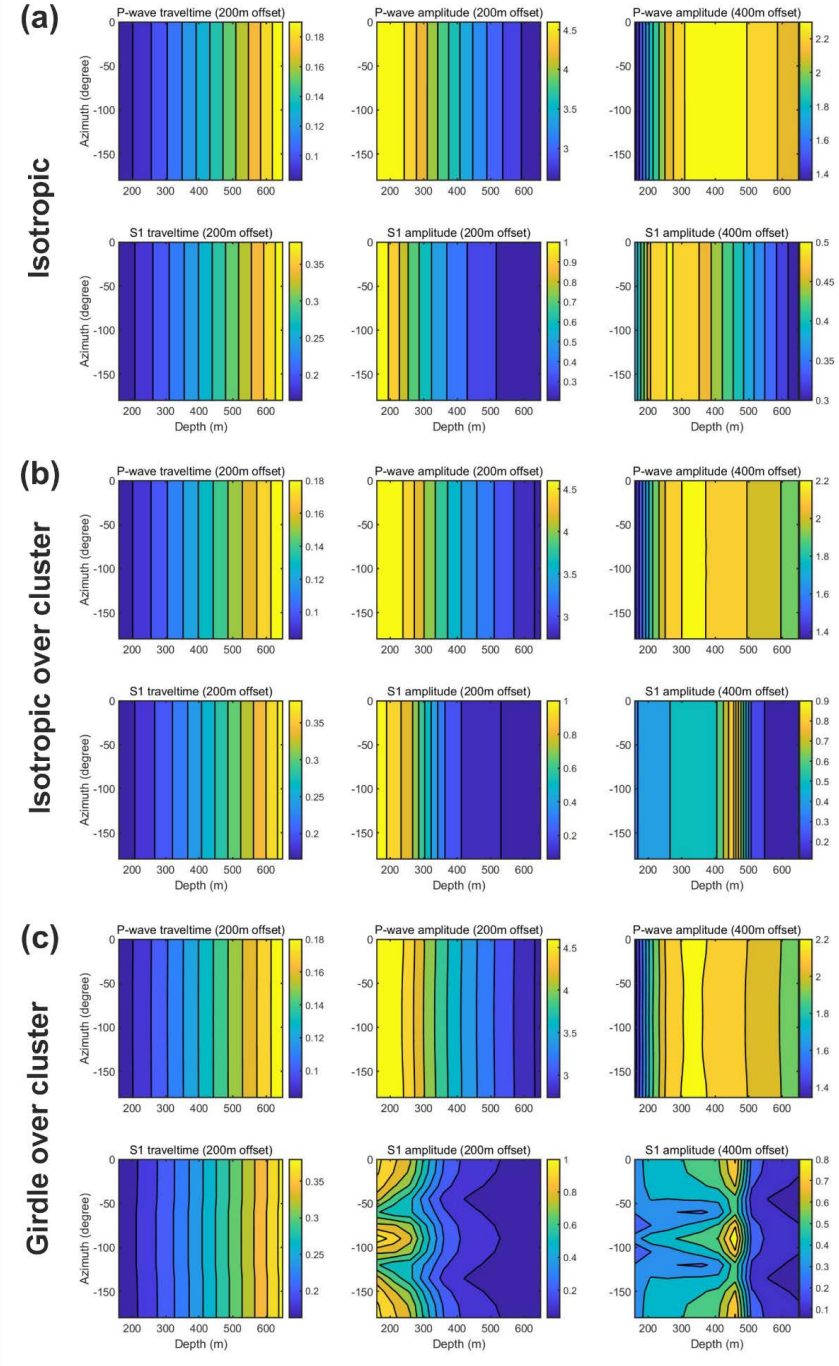

Figure 6: Modelled P-wave and S-wave traveltime and vertical amplitude variation with depth and azimuth (a) isotropic and (b) isotropic with cluster fabric below 230 m, (c) theoretical steady-state ice divide fabric of girdle above strong cluster (Martin et al., 2009). Firn is isotropic in all models and where present the transition to cluster fabric is at 230 m depth. Amplitudes are calculated using the vertical component, consistent with the DAS VSP method.

https://doi.org/10.5194/tc-2021-1
Preprint. Discussion started: 28 January 2021

6 Discussion

Measurements of englacial fabric at Antarctic ice rises have the potential to help constrain recent ice sheet history. DAS VSP data and modelling results presented here highlight the potential of the method to improve our understanding of englacial fabric and therefore recent ice flow history.

Seismic velocities measured in the lower half of the ice column at SIR are high and indicate the likely presence of a strong vertical cluster fabric, consistent with models of fabric formation at ice rises. Observed relatively high amplitude S-waves from far offset shots are also consistent with the presence of englacial fabric. Uncertainties are however too high to establish the depth or azimuthal dependence of anisotropy. A cluster fabric within the lower section of the ice column is consistent with ongoing ice divide flow and fabric formation mechanisms (Martin et al., 2009). The time required to form characteristic fabrics at ice divides is a function of the accumulation rate and ice thickness and as such varies widely. Stable flow over sufficient time is required to form the characteristic fabric. However, the low strain rate at ice rises also allows remnant fabric from a previous flow regime to persist (Brisbourne et al., 2019). The presence of a cluster fabric at depth is therefore not a conclusive indicator of long-term stable flow. Further data are required to investigate the presence of azimuthally variant fabric, for example, that may form under different flow regimes.

Where more reliable measurements are available, the conversion of apparent to true velocity will require an estimate of fabric to account for velocity variation; the deviation of the raypath from the vertical will be a function of both fabric and source-receiver geometry. A correction will be required to account for the fabric-induced difference in velocity between the raypath and the vertical. This is likely best posed as an inversion problem.

Our measured value of Q is low, indicating higher attenuation than previous field measurements in polar ice at similar temperatures, e.g. Q=400-670 at -14° to -25° C (Bentley, 1971) and Q=130-355 at -15° to -22° C (Peters et al., 2012). By invoking transformations to account for measurement frequency, impurity uptake from the mother solution and conversion from flexural vibration to acoustic seismic P-waves, Bentley and Kohnen (1976) demonstrated consistency between field measurements of seismic attenuation and the laboratory measurements of Kuroiwa (1964). However, the same laboratory measurements highlight the sensitivity of seismic attenuation to temperature, impurity concentration and signal frequency. An approximately exponential variation in attenuation occurs at temperatures close to the melting point (above -30°C) across all frequencies. Similarly, samples of ice from Antarctica and Greenland exhibit different behaviour to laboratory-generated samples in the temperature range -20° to -10° C. Laboratory measurements of internal friction at 4 to 9 Hz on the Mizuho ice core (Nakamura and Abe, 1978) also highlight sensitivity to temperature to the melting point and, in contrast to the measurements of Kuroiwa (1964), high degrees of internal friction are observed, equivalent to Q values as low as 10.

It is important to recognise that a number of mechanisms cause attenuation. Field derived measurements provide an estimate of effective Q, the sum of intrinsic Q (e.g. material properties) and apparent Q (e.g. scattering). Decoupling the effects of intrinsic absorption from scattering (perhaps due to impurities or variations in ice crystal size or fabric) will be difficult without further information (e.g., derived from core). For example, Kuroiwa (1964) highlights the significance of grain boundaries and impurities in polycrystalline ice, which results in sensitivity to temperature close to the melting point. Similarly, using the flexural vibration method, Oguro et al. (1982) demonstrated that internal friction varies by up to a factor of five depending on the orientation with respect to the c-axis of a single ice crystal. Additional in situ measurements are therefore required to understand better these sensitivities. This requirement if highlighted by the microstructural analysis of the EPICA DML ice core (European Project for Ice Coring in Antarctica in Dronning Maud Land). There, grain size generally increases with depth but is strongly affected by the impurity content of ice from different climatic stages resulting in a step-change in grain size at depth (Weikusat et al., 2017), highlighting the shortcomings of attenuation profiles based on incomplete parameterisation.

https://doi.org/10.5194/tc-2021-1
Preprint. Discussion started: 28 January 2021

Our measurements are unusual in that in situ measurements of temperature across the entire ice column are available: most seismic attenuation measurements acquired to date are not coincident with a measured profile of englacial temperature or physical properties of the ice. Furthermore, at Skytrain, the ice core will allow for measurements of impurity levels and potentially grain size, providing context to our field measurements. For example, mean NaCl levels in the Skytrain ice core are low (R. Mulvaney, pers. comm.), with concentrations below the lowest levels tested by Kuroiwa (1964), approximating pure ice for these purposes.

Unlike the DAS VSP observations of Booth et al. (2020), where direct P-wave spectra are consistent over a range of depths, significant energy loss with depth is apparent in our observations (Fig. 5c,d). Although the spectral ratio analysis method demonstrates that our attenuation measurement is robust, we cannot rule out the influence on these measurements of the fibre optic cable hanging in the borehole, potentially resulting in a form of signal amplitude reduction unrelated to ice properties. For example, is the uniformity of the coupling or behaviour of the cable influenced by the difference in hydrostatic head of drilling fluid above the sampled range? We therefore regard the signal loss as a robust observation but advocate further experiments to determine the cause of the high degree of attenuation.

7 Recommendations

We combine our field experience, data analysis and modelling results to make a number of recommendations to assist in future experiment design using DAS technology in polar borehole settings.

(1) Unlike at high strain-rate locations or in temperate ice, closure of boreholes at Antarctic ice rises can take a number of years. Achieving a frozen-in, and therefore well-coupled, cable is therefore not always possible in the time available. A method is required to improve coupling between the fibre and the borehole wall. This may mean that the seismic experiment needs to be undertaken whilst drilling fluid is present in the hole or backfilling of the hole undertaken.
(2) Although data acquired with the hammer and plate seismic source demonstrate the feasibility of the DAS method, and have been demonstrated as viable where the fibre optic cable is well-coupled (Booth et al., 2020), a more energetic source (e.g., explosives) would increase the signal to noise ratio and improve the analysis capability beyond that demonstrated here.
(3) Using a geophone and data logger located adjacent to the hammer plate proved to be adequate for estimating source time in this experiment. However, improved timing accuracy is possible with either direct trigger of the DAS recording unit or higher sampling rate of the geophone adjacent to the source. Alternatively, if using an explosive source, we recommend a GPS-synchronised trigger in parallel with GPS timing on the interrogator.
(4) A ruggedised interrogator unit would reduce complexity of the acquisition process (e.g., tolerance to temperature; ruggedized user interface; tolerance to unplanned power outage with automatic restart). An interrogator with low power consumption, or a substantial solar power system, would enable the use of battery power and thus remove the noise source of the generator. In this case, if the interrogator unit requires mains power (110 or 240 V AC) then an inverter is required, the use of which needs to be carefully managed in polar environments to protect both the user and the instrument.
(5) This experiment utilised a multimode fibre cable deployed specifically for DTS measurements. However, it is now standard to deploy bundles of both multi-mode and single-mode cable and this should utilised for all future deployments.
(6) Modelling of the seismic response to likely fabric configurations will optimise field acquisition. Although amplitude variation is a key diagnostic in the scenarios tested here, stronger fabrics may result in measureable traveltime variation for example.
(7) Modelling results for likely ice rise fabric indicate that S-wave amplitude variations are the key diagnostic with the seismic method. As such, a reliable S-wave seismic source is essential. Reliance on P-wave traveltime and amplitude variation

https://doi.org/10.5194/tc-2021-1
Preprint. Discussion started: 28 January 2021

will limit the capacity of the observations to constrain fabric. To what degree an explosive source will be effective remains to be tested. As variation in seismic amplitude is a key diagnostic for constraining fabric geometry, coupling to the borehole to attain consistent amplitude measurements along the length of the cable is therefore critical.

(8) Additional data, such as polarimetric radar measurements or a three-component geophone surface array may improve uniqueness of any interpretation. The deployment of additional fibre optic cable along the surface will complement downhole observations at little logistical overhead. However, measurements using surface-deployed cable will be limited to horizontal longitudinal strain rate and further modelling will be required to explore the benefit of this additional information in such scenarios. With a single fibre optic cable for both downhole and surface measurements, only a single interrogator unit is necessary.

8 Conclusions

We have demonstrated the feasibility and potential of DAS measurements in Antarctic settings using existing infrastructure. This presents opportunities for relatively low-cost and logistically light experiments, both adding value to existing studies and opening opportunities for continent-wide experiments at relatively low risk. We have presented results from a walkaway VSP acquired at SIR. Estimates of seismic velocity (4029 ± 244 m s^{-1}) in the lower section of the ice column are consistent with a cluster fabric. Relatively high S-wave amplitudes from far-offset shots are also consistent with the presence of fabric. Estimates of Q in the same interval (75 ± 12) are lower than previous estimates of attenuation in ice. Our data lack the signal strength required to allow a more detailed interpretation of the structure at SIR. However, observations of direct and reflected seismic waves from a low-energy hammer source at a range of offsets and azimuths underscore the potential of the DAS method to investigate englacial and basal structure in similar settings. Modelling of the effect of likely ice fabric geometries on P- and S-wave traveltimes and amplitudes demonstrates the potential for this method to identify and discriminate ice fabric at ice rises. The results of this pilot study present an opportunity to improve the design of future experiments and we make a number of recommendations related to both acquisition design, instrumentation and field methodology.

Data availability

Data have been submitted to the Polar Data Centre at https://www.bas.ac.uk/data/uk-pdc/ for public access.

Author contribution

AB and MK designed and led the experiment with support from SK and AS. MK conducted data acquisition with support from AB and SK. AB undertook data analysis with assistance from MK, TH and SK. AB wrote the manuscript with contributions from all others.

Competing interests

The authors declare no competing interests.

Acknowledgements

We are grateful to Anne Flink, BAS Operations and Rothera Station personnel who supported this experiment. Athena Chalari and Andy Clarke at Silixa Ltd loaned equipment, assisted with planning and provided technical support. Fieldwork was undertaken as part of the BEAMISH Project (NERC AFI award numbers NE/G014159/1). JMK was supported by additional

funding from NERC award CASS-166. The Skytrain borehole and fibre optic cable are part of the University of Cambridge WACSWAIN Project (EU Horizon 2020 agreement No. 742224). We thank the Computational Infrastructure for Geodynamics (http://geodynamics.org) which is funded by the National Science Foundation under awards EAR-0949446 and EAR-1550901.

References

Baird, A. F., Kendall, J. M., Fisher, Q. J., and Budge, J.: The Role of Texture, Cracks, and Fractures in Highly Anisotropic Shales, Journal of Geophysical Research: Solid Earth, 122, 10,341-310,351, 10.1002/2017jb014710, 2017.

Barletta, V. R., Bevis, M., Smith, B. E., Wilson, T., Brown, A., Bordoni, A., Willis, M., Khan, S. A., Rovira-Navarro, M., Dalziel, I., Smalley, R., Kendrick, E., Konfal, S., Caccamise, D. J., Aster, R. C., Nyblade, A., and Wiens, D. A.: Observed rapid bedrock uplift in Amundsen Sea Embayment promotes ice-sheet stability, Science, 360, 1335-1339, 10.1126/science.aao1447, 2018.

Bath, M.: Spectral analysis in geophysics, in: Developments in Solid Earth Geophysics, Elsevier, Amsterdam, 415, 1974.

Bentley, C. R.: Seismic Evidence for Moraine within the Basal Antarctic Ice Sheet, in: Antarctic Snow and Ice Studies II, Antarctic Research Series, 89-129, 1971.

Bentley, C. R., and Kohnen, H.: Seismic refraction measurements of internal friction in Antarctic ice, J. Geophys. Res., 81, 1519-1526, 10.1029/JB081i008p01519, 1976.

Bingham, R. G., Rippin, D. M., Karlsson, N. B., Corr, H. F. J., Ferraccioli, F., Jordan, T. A., Le Brocq, A. M., Rose, K. C., Ross, N., and Siegert, M. J.: Ice-flow structure and ice dynamic changes in the Weddell Sea sector of West Antarctica from radar-imaged internal layering, J. Geophys. Res.-Earth, 120, 655-670, 10.1002/2014jf003291, 2015.

Booth, A. D., Christoffersen, P., Schoonman, C., Clarke, A., Hubbard, B., Law, R., Doyle, S. H., Chudley, T. R., and Chalari, A.: Distributed Acoustic Sensing of Seismic Properties in a Borehole Drilled on a Fast-Flowing Greenlandic Outlet Glacier, Geophys. Res. Lett., 47, e2020GL088148, 10.1029/2020gl088148, 2020.

Bradley, S. L., Hindmarsh, R. C. A., Whitehouse, P. L., Bentley, M. J., and King, M. A.: Low post-glacial rebound rates in the Weddell Sea due to Late Holocene ice-sheet readvance, Ear. Planet. Sci. Let., 413, 79-89, 10.1016/j.epsl.2014.12.039, 2015.

Brisbourne, A. M., Martín, C., Smith, A. M., Baird, A. F., Kendall, J. M., and Kingslake, J.: Constraining Recent Ice Flow History at Korff Ice Rise, West Antarctica, Using Radar and Seismic Measurements of Ice Fabric, J. Geophys. Res.:Earth Surf., 124, 175-194, 10.1029/2018jf004776, 2019.

Dasgupta, R., and Clark, R. A.: Estimation of Q from surface seismic reflection data, Geophysics, 63, 2120-2128, 10.1190/1.1444505, 1998.

Dean, T., Cuny, T., and Hartog, A. H.: The effect of gauge length on axially incident P-waves measured using fibre optic distributed vibration sensing, Geophysical Prospecting, 65, 184-193, 10.1111/1365-2478.12419, 2017.

Griffiths, L. J., Smolka, F. R., and Trembly, L. D.: Adaptive Deconvolution: A New Technique for Processing Time-Varying Seismic Data, Geophysics, 42, 742-759, 10.1190/1.1440743, 1977.

Guest, W. S., and Kendall, J. M.: Modelling seismic waveforms in anisotropic inhomogeneous media using ray and Maslov asymptotic theory: application to exploration seismology, Can. J. Explor. Geophys., 29, 78-92, 1993.

Harland, S., Kendall, J., Stuart, G., Lloyd, G., Baird, A., Smith, A., Pritchard, H., and Brisbourne, A.: Deformation in Rutford Ice Stream, West Antarctica: measuring shear-wave anisotropy from icequakes, Ann. Glaciol., 54, 105-114, 2013.

Hartog, A. H.: An introduction to distributed optical fibre sensors, CRC Press/Taylor and Francis, Boca Raton, Florida, 2017.

Hillenbrand, C. D., Bentley, M. J., Stolldorf, T. D., Hein, A. S., Kuhn, G., Graham, A. G. C., Fogwill, C. J., Kristoffersen, Y., Smith, J. A., Anderson, J. B., Larter, R. D., Melles, M., Hodgson, D. A., Mulvaney, R., and Sugden, D. E.: Reconstruction of changes in the Weddell Sea sector of the Antarctic Ice Sheet since the Last Glacial Maximum, Quat. Sci. Rev., 100, 111-136, 10.1016/j.quascirev.2013.07.020, 2014.

IPCC: Climate Change 2013: The Physical Science Basis. Contribution of Working Group I to the Fifth Assessment Report of the Intergovernmental Panel on Climate Change, Cambridge University Press, Cambridge, United Kingdom and New York, NY, USA, 1535, 2013.

Kendall, J.-M., and Thomson, C. J.: A comment on the form of the geometrical spreading equations, with some numerical examples of seismic ray tracing in inhomogeneous, anisotropic media, Geophys. J. Int., 99, 401-413, 10.1111/j.1365-246X.1989.tb01697.x, 1989.

Kingslake, J., Martin, C., Arthern, R. J., Corr, H. F. J., and King, E. C.: Ice-flow reorganization in West Antarctica 2.5kyr ago dated using radar-derived englacial flow velocities, Geophys. Res. Lett., 43, 9103-9112, 10.1002/2016gl070278, 2016.

Kingslake, J., Scherer, R. P., Albrecht, T., Coenen, J., Powell, R. D., Reese, R., Stansell, N. D., Tulaczyk, S., Wearing, M. G., and Whitehouse, P. L.: Extensive retreat and re-advance of the West Antarctic Ice Sheet during the Holocene, Nature, 558, 430-434, 10.1038/s41586-018-0208-x, 2018.

Kuroiwa, D.: Internal Friction of Ice. Ⅰ; The Internal Friction of H2O and D2O Ice, and the Influence of Chemical Impurities on Mechanical Damping, Contributions from the Institute of Low Temperature Science, 18, 1-37, 1964.

Larour, E., Seroussi, H., Adhikari, S., Ivins, E., Caron, L., Morlighem, M., and Schlegel, N.: Slowdown in Antarctic mass loss from solid Earth and sea-level feedbacks, Science, 364, eaav7908, 10.1126/science.aav7908, 2019.

Martin, C., Gudmundsson, G. H., Pritchard, H. D., and Gagliardini, O.: On the effects of anisotropic rheology on ice flow, internal structure, and the age-depth relationship at ice divides, J. Geophys. Res.-Earth, 114, 10.1029/2008jf001204, 2009.

Mercer, J. H.: West Antarctic ice sheet and CO2 greenhouse effect: a threat of disaster, Nature, 271, 321-325, 1978.

Mulvaney, R., Rix, J., and Polfrey, S.: The WACSWAIN ice drilling project, Ann. Glaciol., In review, 2020.

Nakamura, T., and Abe, O.: Internal friction of Antarctic Mizuho ice cores at low frequency, Mem. Natl. Inst. Polar Res. (Jpn.), 10, 102-113, 1978.

Oguro, M., Hatano, K., and Kato, S.: Orientation dependence of internal friction in artificial single crystals of ice, Cold Reg. Sci. Tech., 6, 29-35, https://doi.org/10.1016/0165-232X(82)90042-8, 1982.

Peters, L. E., Anandakrishnan, S., Alley, R. B., and Voigt, D. E.: Seismic attenuation in glacial ice: A proxy for englacial temperature, J. Geophys. Res.-Earth, 117, Artn F02008 10.1029/2011jf002201, 2012.

Rignot, E., Mouginot, J., and Scheuchl, B.: Ice Flow of the Antarctic Ice Sheet, Science, 333, 1427-1430, 10.1126/science.1208336, 2011.

Rignot, E., Mouginot, J., Scheuchl, B., van den Broeke, M., van Wessem, M. J., and Morlighem, M.: Four decades of Antarctic Ice Sheet mass balance from 1979–2017, Proc. Nat. Acad. Sci., 116, 1095-1103, 10.1073/pnas.1812883116, 2019.

Ross, N., Bingham, R. G., Corr, H. F. J., Ferraccioli, F., Jordan, T. A., Le Brocq, A., Rippin, D. M., Young, D., Blankenship, D. D., and Siegert, M. J.: Steep reverse bed slope at the grounding line of the Weddell Sea sector in West Antarctica, Nat. Geosci., 5, 393-396, 10.1038/ngeo1468, 2012.

Scambos, T. A., Haran, T. M., Fahnestock, M. A., Painter, T. H., and Bohlander, J.: MODIS-based Mosaic of Antarctica (MOA) data sets: Continent-wide surface morphology and snow grain size, Remote Sens. Environ., 111, 242-257, 10.1016/j.rse.2006.12.020, 2007.

Shepherd, A., Ivins, E., Rignot, E., Smith, B., van den Broeke, M., Velicogna, I., Whitehouse, P., Briggs, K., Joughin, I., Krinner, G., Nowicki, S., Payne, T., Scambos, T., Schlegel, N., A, G., Agosta, C., Ahlstrøm, A., Babonis, G., Barletta, V., Blazquez, A., Bonin, J., Csatho, B., Cullather, R., Felikson, D., Fettweis, X., Forsberg, R., Gallee, H., Gardner, A., Gilbert, L., Groh, A., Gunter, B., Hanna, E., Harig, C., Helm, V., Horvath, A., Horwath, M., Khan, S., Kjeldsen, K. K., Konrad, H., Langen, P., Lecavalier, B., Loomis, B., Luthcke, S., McMillan, M., Melini, D., Mernild, S., Mohajerani, Y., Moore, P., Mouginot, J., Moyano, G., Muir, A., Nagler, T., Nield, G., Nilsson, J., Noel, B., Otosaka, I., Pattle, M. E., Peltier, W. R., Pie, N., Rietbroek, R., Rott, H., Sandberg-Sørensen, L., Sasgen, I., Save, H., Scheuchl, B., Schrama, E., Schröder, L., Seo, K.-W., Simonsen, S., Slater, T., Spada, G., Sutterley, T., Talpe, M., Tarasov, L., van de Berg, W. J., van der Wal, W., van Wessem,

https://doi.org/10.5194/tc-2021-1
Preprint. Discussion started: 28 January 2021

M., Vishwakarma, B. D., Wiese, D., Wouters, B., and The, I. t.: Mass balance of the Antarctic Ice Sheet from 1992 to 2017, Nature, 558, 219-222, 10.1038/s41586-018-0179-y, 2018.

Siegert, M., Ross, N., Corr, H., Kingslake, J., and Hindmarsh, R.: Late Holocene ice-flow reconfiguration in the Weddell Sea sector of West Antarctica, Quat. Sci. Rev., 78, 98-107, 10.1016/j.quascirev.2013.08.003, 2013.

505 Siegert, M. J., Kingslake, J., Ross, N., Whitehouse, P. L., Woodward, J., Jamieson, S. S. R., Bentley, M. J., Winter, K., Wearing, M., Hein, A. S., Jeofry, H., and Sugden, D. E.: Major Ice Sheet Change in the Weddell Sea Sector of West Antarctica Over the Last 5,000 Years, Rev. Geophys., 57, 1197-1223, 10.1029/2019rg000651, 2019.

Tromp, J., Komattisch, D., and Liu, Q.: Spectral-Element and Adjoint Methods in Seismology, Communications in Computational Physics, 3, 2008.

510 Walter, F., Gräff, D., Lindner, F., Paitz, P., Köpfli, M., Chmiel, M., and Fichtner, A.: Distributed acoustic sensing of microseismic sources and wave propagation in glaciated terrain, Nat. Commun., 11, 2436, 10.1038/s41467-020-15824-6, 2020.

Wearing, M. G., and Kingslake, J.: Holocene Formation of Henry Ice Rise, West Antarctica, Inferred From Ice-Penetrating Radar, J. Geophys. Res.:Earth Surf., 124, 2224-2240, 10.1029/2018jf004988, 2019.

515 Weikusat, I., Jansen, D., Binder, T., Eichler, J., Faria, S. H., Wilhelms, F., Kipfstuhl, S., Sheldon, S., Miller, H., Dahl-Jensen, D., and Kleiner, T.: Physical analysis of an Antarctic ice core-towards an integration of micro- and macrodynamics of polar ice, Philosophical transactions. Series A, Mathematical, physical, and engineering sciences, 375, 10.1098/rsta.2015.0347, 2017.